BIAS IMPACT ANALYSIS AND CALIBRATION OF UAV-BASED MOBILE LIDAR SYSTEM

*Tamer Shamseldin, Radhika Ravi, Magdy Elbahnasawy, Yun-Jou Lin, and Ayman Habib**

Lyles School of Civil Engineering, Purdue University, USA

ABSTRACT

Over the past few years, developments in mobile mapping technology, specifically Unmanned Aerial Vehicles (UAVs), have made accurate 3D mapping more feasible, thus emerging as an economical and practical mobile mapping platform. LiDAR-based UAV mapping systems are gaining widespread recognition as an efficient and cost-effective technique for rapid collection of 3D geospatial data. To derive point clouds with high positional accuracy, estimation of mounting parameters relating the laser scanners to the onboard GNSS/INS unit is the foremost and necessary step. In this paper, we first devise an optimal flight and target configuration by conducting a rigorous theoretical analysis of the potential impact of bias in mounting parameters of a LiDAR unit on the resultant point cloud. Then, we propose a LiDAR system calibration strategy that can directly estimate the mounting parameters for spinning multi-beam laser scanners onboard a UAV through an outdoor calibration procedure.

Index Terms— LiDAR, UAV, GNSS/INS, multi-beam laser scanners, mounting parameters

1. INTRODUCTION

3D geospatial data is rapidly gaining popularity due to its contribution to a variety of applications such as Digital Building Model (DBM) generation, telecommunications, infrastructure monitoring, transportation corridor asset management, and crash/accident scene reconstruction [1], [2]. Recent advances in hardware and software development have made it possible to conduct accurate 3D mapping without using costly and high-end data acquisition systems. For example, low-cost laser scanners, such as Velodyne units, and navigation systems can provide accurate mapping if they are properly integrated at the hardware and software levels and accurately calibrated.

Over the past few years, many research efforts have been devoted to modeling the inherent systematic errors in Velodyne laser scanners as well as the calibration of LiDAR systems to estimate the internal sensor characteristics and mounting parameters [3], [4]. [5] performed a geometric calibration with stationary VLP-16 to marginally improve the accuracy of the point clouds by approximately 20%. Moreover, the authors also investigated the range accuracy of VLP-16, which is quoted to have a Root Mean Square Error (RMSE) value between 22 and 27 mm in the factory supplied calibration certificate. But, it was observed that some of the laser beams have worse range accuracy than others. Although many LiDAR system calibration procedures have been developed in the past, outdoor calibration of integrated GNSS/INS and multi-unit 3D laser scanners is still an active area of research.

The major contribution of this work is to develop a LiDAR system calibration strategy for a UAV-based mobile mapping system that can directly estimate the mounting parameters for spinning multi-beam laser scanners through an outdoor calibration procedure. This approach is based on the use of conjugate planar/linear features in overlapping point clouds derived from different flight lines. Designing an optimal configuration for calibration is the first and foremost step in order to ensure the most accurate estimates of mounting parameters. This is achieved by conducting a rigorous theoretical analysis of the potential impact of bias in mounting parameters of a LiDAR unit on the resultant point cloud. This can be achieved through a bias impact analysis that evaluates the effect of biases in the mounting on features with different configurations. The dependency of the impact on the orientation of target primitives and relative flight line configuration would help in deducing the configuration that would maximize as well as decouple the impact of bias in each mounting parameter, i.e., the lever-arm and boresight angles, so as to ensure their accurate estimation. The proposed calibration strategy is validated by calibrating a UAV-based LiDAR system using the data acquired according to the experimental configuration proposed based on the bias impact analysis. The performance of calibration is evaluated by analyzing the a-posteriori variance factor of the Least Squares Adjustment (LSA) procedure and the quality of fit of the adjusted point cloud to planar/linear features before and after the calibration process.

2. SYSTEM INTEGRATION

To ensure that the UAV system will be capable of satisfying the needs of mapping and monitoring activities, the specifications of each individual component should be investigated, i.e., whether they are commensurate with payload restrictions as well as the extent of the area to be mapped, and required accuracy. The DJI M600 UAV is selected as a promising platform, which allows around 6 kg payload of sensors/equipment to be installed onboard. This system includes a navigation unit and one LiDAR sensor. These components are rigidly fixed within the UAV platform as shown in Figure 1.

Generally, the manipulation of the collected LiDAR data requires the direct georeferencing of the mapping platform, which can be established by deriving the platform's position

Acknowledgment: This work was supported in part by the Advanced Research Projects Agency-Energy, U.S. Department of Energy, under Award Number DE-AR0000593.

and orientation using an integrated GNSS/INS system [6]. For this investigation, the Applanix APX-15 UAV is considered due to its low weight, compact size, and precise positioning and orientation information. In post-processing mode, it can attain an accuracy of 0.025º for pitch/roll and 0.08º for heading (yaw), and the position accuracy is 0.02-0.05 m [7]. The LiDAR unit used in this research is a Velodyne VLP-16 Puck HI-RES. It is a small LiDAR unit, which has 16 lasers beams that are aligned over the range of +10.00º to -10.00º that provides the vertical field of view, and it delivers a 360º horizontal field of view. As the LiDAR unit can be mounted at any random configuration according to the application, the vertical and horizontal field of view are stated with respect to the LiDAR unit coordinate system. It can scan up to 300,000 points per second with a range of 100 meters and typical accuracy of ± 3 cm [8]. For storing the collected data, a Raspberry Pi 3 with 1.2 GHz 64-bit quad-core ARMv8 CPU is used with around 50 gm weight. Its small size and light weight eases its installation on the UAV. In order to derive direct georeferencing data, the APX-15 supplies sequentially precise time pulses, known as pulse-per-second (PPS) signals, which gives the ability to generate a time-tagged point cloud. Furthermore, the APX-15 provides a navigation message, also known as GPRMC message (including information regarding position, rotation, and GPS time), which is recorded over a dedicated RS-232 serial port and received by the LiDAR unit via the interface box in the form of serial data.

Fig. 1. UAV-based mapping system configuration

3. BIAS IMPACT ANALYSIS

In this section, we provide an overview of the theoretical analysis conducted for a UAV-based LiDAR system consisting of a GNSS/INS unit and a multi-beam spinning laser unit. Starting with the 3D point positioning equation, we derive the impact of bias in the mounting parameters by analyzing the partial derivatives of the 3D mapping frame coordinates with respect to each of the parameters. Equation 1 states the 3D point positioning equation used to derive the coordinates in the mapping frame for the points scanned by the LiDAR unit. The terms involved in the equation are depicted in Figure 2.

For simplifying the analysis without any loss of generality, we assume a vertical system, i.e., the z-axis of the IMU body frame, which is ordinated with the platform, is perfectly aligned with the vertical direction of the mapping frame. Note that the IMU xy-axes are aligned along the starboard and forward directions, respectively. Also, we assume that the flight line directions are either from South-to-North ($\kappa = 0°$) or from North-to-South ($\kappa = 180°$). These assumptions facilitate the decision as to whether the impact is along/across the flight line and vertical directions. As a result, the rotation matrix $R_b^m(t)$ would be given by Equation 2, where the top and bottom signs are for S-N and N-S flight line directions, respectively. The partial derivatives of Equation 1 with respect to the lever arm (ΔX, ΔY, and ΔZ) and boresight angles ($\Delta\omega$, $\Delta\phi$, $\Delta\kappa$) are given by Equation 3, where (x, y, z) denote the coordinates of the point relative to the laser unit coordinate system. Note that ΔX, ΔY, and ΔZ denote the lever arm components across flight, along flight, and vertical directions, respectively. Similarly, $\Delta\omega$, $\Delta\phi$, and $\Delta\kappa$ denote the boresight pitch, roll, and heading, respectively.

The vector and matrix notations used in this paper are as follows:

- $\boldsymbol{r_a^b}$ denotes the coordinates of point 'a' relative to point 'b' in the coordinate system associated with point 'b'.
- $\boldsymbol{R_a^b}$ denotes the rotation matrix that transforms a vector defined relative to the coordinate system 'a' into a vector defined relative to the coordinate system 'b'.

$$r_I^m = r_b^m(t) + R_b^m(t)\, r_{lu}^b + R_b^m(t)\, R_{lu}^b\, r_l^{lu}(t) \quad (1)$$

$$R_b^m(t) = \begin{bmatrix} \pm 1 & 0 & 0 \\ 0 & \pm 1 & 0 \\ 0 & 0 & 1 \end{bmatrix} \quad (2)$$

$$\delta r_I^m{}_{(\delta\Delta X,\, \delta\Delta Y,\, \delta\Delta Z,\, \delta\Delta\omega,\, \delta\Delta\phi,\, \delta\Delta\kappa)} = \begin{bmatrix} \pm\delta\Delta X \\ \pm\delta\Delta Y \\ \delta\Delta Z \end{bmatrix} + \begin{bmatrix} \pm z\,\delta\Delta\phi \mp y\,\delta\Delta\kappa \\ \mp z\,\delta\Delta\omega \pm x\,\delta\Delta\kappa \\ y\,\delta\Delta\omega - x\,\delta\Delta\phi \end{bmatrix} \quad (3)$$

Conducting an in-depth analysis by isolating the terms in Equation 3 results in the following assessment of the impact of bias in each of the system mounting parameters:

Impact of Bias in Lever-arm component across the flying direction (ΔX): A bias in this component ($\delta\Delta X$) will introduce a constant shift ($\pm\,\delta\Delta X$) across the flying direction. The introduced shift is flying direction dependent and does not depend on the location of the point in question relative to the laser beam firing point. As a result, its impact will be visible in case of vertical planes parallel to the flying direction scanned from two flight lines in opposite directions.

Impact of Bias in Lever-arm component along the flying direction (ΔY): A bias in this component ($\delta\Delta Y$) will introduce a constant shift ($\pm\,\delta\Delta Y$) along the flying direction. The introduced shift is flying direction dependent and does not depend on the location of the point in question relative to the laser beam firing point. Again, it would impact vertical planes perpendicular to the flying direction scanned from two flight lines in opposite directions.

Impact of Bias in Lever-arm component in the vertical direction (ΔZ): A bias in this component ($\delta\Delta Z$) will introduce a constant shift ($\delta\Delta Z$) in the vertical direction. The introduced shift is flying direction independent and does not depend on the location of the point in question relative to the laser beam firing point. As a result, the entire point cloud would be shifted in the vertical direction by the same amount. So, this bias would not affect planes in any of the orientations for any flight line configuration.

Impact of Bias in Boresight Pitch ($\Delta\omega$): A bias in this component ($\delta\Delta\omega$) will cause shifts along the flying direction as well as in the vertical direction. The impact along the flying direction ($\mp\, z\,\delta\Delta\omega$) is flying direction dependent and its magnitude depends on the height (z) of the point in question relative to the laser beam firing point. This impact would be visible in case of a planar feature perpendicular to the flying direction being scanned by flight lines in opposite directions. Since a bias in lever arm (ΔY) also affects similarly oriented

planes, there is a need to decouple the impacts so as to estimate both these biases accurately. A detailed analysis reveals that this can be achieved either by having flight lines at different flying heights or having a significant variation in target height with respect to the flying height. The impact of boresight pitch bias in the vertical direction ($y\ \delta\Delta\omega$) would be manifested in horizontal planes. The magnitude of this impact depends on the y-coordinate of the point in question. So, this impact would be visible even in case of a single flight line capturing a horizontal planar feature. Note that such an impact should also aid in decoupling $\delta\Delta\omega$ and $\delta\Delta Y$, provided there is a significant y-coordinate variability. In this study, since the FOV of the LiDAR unit is ±10º, the y-coordinate variability is not enough to eliminate the correlation.

Impact of Bias in Boresight Roll ($\Delta\phi$): A bias in this component ($\delta\Delta\phi$) will cause shifts across the flying direction as well as in the vertical direction. The impact of this bias across the flying direction ($\pm\ z\ \delta\Delta\phi$) is flying direction dependent and its magnitude depends on the height (z) of the point in question relative to the laser beam firing point. This bias would impact vertical planes parallel to the flying direction scanned from two flight lines in opposite directions. Since a bias in lever arm ΔX also affects similarly oriented planes, there is a need to decouple the impacts so as to estimate both these biases accurately. Again, a detailed analysis reveals that this can be achieved either by having flight lines at different flying heights or having a significant variation in target height with respect to the flying height. The magnitude of the impact of this bias in the vertical direction ($-x\ \delta\Delta\phi$) depends on the x-coordinate of the point in question. Since the x-coordinate would change signs depending on the flying direction, this impact would be flying direction dependent. A detailed assessment reveals that this bias would cause a discrepancy for horizontal planes scanned from two flight lines in the same direction depending on the lateral distance between the tracks. On the other hand, for two tracks in opposite directions, the discrepancy would depend on the lateral location of the planar patch of interest relative to the bisecting direction between the tracks.

Impact of Bias in Boresight Heading ($\Delta\kappa$): A bias in this component ($\delta\Delta\kappa$) will cause shifts across and along the flying direction. The impact of this bias across the flying direction ($\mp\ y\ \delta\Delta\kappa$) is dependent on the y-coordinate variability. So, this would cause a discrepancy for the vertical planes parallel to the flying direction for a single track. Moreover, the discrepancy on combining two tracks in same or opposite directions would depend on the $\pm y$ variability within the points comprising the planes.

The impact of this bias along the flying direction ($\pm\ x\ \delta\Delta\kappa$) is flying direction independent but x-coordinate dependent. This bias would induce a discrepancy in case of vertical planes perpendicular to the flying direction scanned from two flight lines in the same/opposite directions depending on the lateral distance between the tracks.

Based on the above discussion, the following comments can be made regarding an optimal flight configuration for calibration:

- The lever arm ΔX can be estimated using opposite flight lines while scanning vertical planar features parallel to the flight direction.
- The lever arm ΔY can be estimated using opposite flight lines while scanning vertical planar features perpendicular to the flight direction.
- The lever arm ΔZ for a given spinning multi-beam laser scanner can be estimated only using vertical control.
- The boresight pitch $\Delta\omega$ can be estimated using opposite flight lines along with another flight line at a different height while scanning horizontal planar features and vertical planar features perpendicular to the flight direction. Another alternative for having a flight line at different flying height is to have vertical planar features with significant height variability w.r.t. the flying height.
- The boresight roll $\Delta\phi$ can be estimated using opposite flight lines along with another flight line at a different height while scanning horizontal planar features and vertical planar features parallel to the flight direction. Another alternative for having a flight line at different flying height is to have vertical planar features with significant height variability w.r.t. the flying height.

The boresight heading $\Delta\kappa$ can be estimated by scanning vertical planes from two flight lines in the same direction with a significant lateral separation between them. This configuration would eliminate any discrepancies caused by lever-arm components.

4. SYSTEM CALIBRATION

In this section, we propose a strategy to calibrate the mounting parameters of the LiDAR unit with respect to the onboard GNSS/INS unit using geometric tie features (e.g., planar, and linear/cylindrical features). After collecting data from several flight lines, a 3D point cloud relative to a global reference frame will be derived using the GNSS/INS unit position and orientation, and initial estimates for the mounting parameters. Then, conjugate features are identified and extracted from the reconstructed point cloud. Finally, an iterative system calibration with weight modification is proposed to derive the mounting parameters based on the minimization of normal distance between conjugate features. However, conjugate feature extraction from several flight lines could be time-consuming and inefficient, especially when the initial estimates for mounting parameters used to reconstruct the 3D point cloud are considerably inaccurate. To facilitate automated identification of conjugate features in such cases, specifically designed calibration boards covered by highly reflective surfaces, that could be easily deployed and set up in outdoor environments are used. The highly reflective boards can be easily identified from intensity data, as shown in Figure 3, where the points belonging to these boards exhibit higher intensity values compared to other LiDAR points. Note that that the buffer values for linear/planar feature extraction are determined based on the accuracy of initial estimates of the mounting parameters.

The mounting parameters that are derived from calibration are the lever arm ($\Delta X, \Delta Y$) and boresight angles ($\Delta\omega, \Delta\phi, \Delta\kappa$) for the LiDAR unit. The lever arm ΔZ for the LiDAR unit cannot be estimated in the calibration procedure since any change in ΔZ will not introduce discrepancies among the different versions of the same feature captured from different

flight lines. It would only result in a shift of the point cloud in the vertical direction as a whole. So, ΔZ is fixed during the calibration procedure. It is either manually measured or determined using vertical control (such as, horizontal planar patches with known elevation).

When the initial estimate of the mounting parameters is inaccurate, the estimated modified weight matrix would be imprecise which would affect the accuracy of the derived mounting parameters. Hence, this research proposes an iterative calibration procedure. Firstly, the discrepancy among extracted features is minimized to derive mounting parameters through the weight modification process. Then, the points along the extracted features are re-generated using the newly estimated mounting parameters and the discrepancy among conjugate features is minimized again using a newly defined modified weight matrix. The above steps are repeated until the change in the estimates of the mounting parameters is below a predefined threshold.

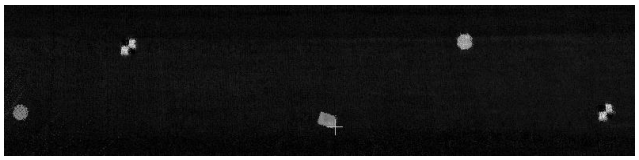

Fig. 3 Intensity data from a point cloud that includes highly reflective boards

5. EXPERIMENTAL RESULTS

The dataset collected by the UAV-based system comprises six flight lines each at fixed heights of 15 m and 25 m above the ground, with different directions and lateral distance between them. These flight lines cover the calibration primitives at an approximate speed of 1.5 m/sec. The calibration procedure estimates the planimetric lever-arm components $(\Delta X, \Delta Y)$ and the boresight angles since the presence of different flying heights would eliminate any correlation among such parameters. However, the vertical lever-arm component (ΔZ) of the laser scanner is fixed. The dataset collected by the UAV-based system covers sixteen specially designed highly reflective boards. Five hut-shaped target boards are also deployed, with their ridges oriented perpendicular to each other. The two surfaces corresponding to each of these huts are used as planar features for calibration, and their ridges are used as conjugate linear features between the overlapping LiDAR point clouds from different flight lines. Four planar rooftops of a shed covered by the flight lines are also used as planar features. All these features ensure enough control along the X, Y, Z-directions. Figure 4 shows a portion of the calibration test field with the calibration primitives circled in red.

The qualitative evaluation of the calibration results is depicted in Figure 5, indicating a significant improvement of checkerboard targets, hut surfaces, and shed rooftops. The initial approximations of all the mounting parameters and the final results (along with their standard deviations) after calibration are listed in Table I, where the parameters highlighted in red are fixed during calibration. The square root of the a-posteriori variance factor $(\hat{\sigma}_o)$ is 2.24 cm after calibration, which represents the average compatibility between all the conjugate and pseudo-conjugate point pairings. This is better than the expected accuracy of around 5-6 cm for a flying height of 15-25 m according to the accuracies of the hardware involved [9]. For quantitative evaluation, the object points derived from the LiDAR unit are used to compute the RMSE of normal distance for each feature using the corresponding line/plane parameters derived before and after calibration. These RMSE values were found to lie in the range of 1.5 to 2.5 cm for all the features.

Fig. 4. UAV-based system: Calibration test field

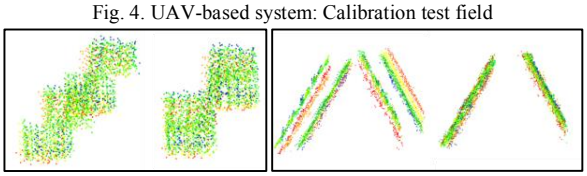

(a) (b)

Fig. 5 Qualitative evaluation of some of the extracted checkerboard targets, hut surfaces, and shed rooftops: (a) before calibration, and (b) after calibration.

TABLE I
MOUNTING PARAMETERS BEFORE AND AFTER CALIBRATION OF THE UAV-BASED SYSTEM

VLP-16 LiDAR Unit Mounting Parameters (r^b_{Lu}) (R^b_{Lu})						
	ΔX (m)	**ΔY (m)**	**ΔZ (m)**	**Δω (°)**	**Δφ (°)**	**Δκ (°)**
Initial	0	0.02	0	0	0	0
Final	0.0180	-0.0067	0	0.1598	-0.6942	-0.2538
Standard Deviation	0.0118	0.0181	Fixed	0.0361	0.0139	0.0438

7. REFERENCES

[1] Lin, Hui, et al. "Semantic decomposition and reconstruction of residential scenes from LiDAR data." *ACM Transactions on Graphics (TOG)* 32.4 (2013): 66.

[2] Puente, I., et al. "Review of mobile mapping and surveying technologies." *Measurement* 46.7 (2013): 2127-2145.

[3] Atanacio-Jiménez,G.;González-Barbosa,J.J.;Hurtado-Ramos, B.;Ornelas-Rodríguez, F.J.; Jiménez-Hernández,H.;García-Ramirez, T.; González-Barbosa, R. Lidar velodyne HDL-64E Calibration using Pattern Planes. Int. J. Adv. Robot. Syst. 2011, 8, 59.

[4] Glennie, C.; Brooks, B.; Ericksen, T.; Hauser, D.; Hudnut, K.; Foster, J.; Avery, J. Compact Multipurpose Mobile Laser Scanning System—Initial Tests and Results. Remote Sens. **2013**, 5, 521–538.

[5] Glennie, C.L.; Kusari, A.; Facchin, A. Calibration and stability analysis of the VLP-16 laser scanner. Int. Arch. Photogramm. Remote Sens. Spat. Inf. Sci. 2016, 40, 55–60.

[6] Chiang, K.-W., Tsai, M.-L., Naser, E.-S., Habib, A., Chu, C.-H., 2015b. New Calibration Method Using Low Cost MEM IMUs to Verify the Performance of UAV-Borne MMS Payloads. Sensors 15, 6560–6585. doi:10.3390/s150306560.

[7] Applanix, 2016. APX-15 UAV Version 2, Single Board GNSS-Inertial Solution, https://www.applanix.com/downloads/products/specs/APX 15_DS_NEW_0408_YW.pdf (Accessed 08 Oct 2017).

[8] Velodyne, 2016. Velodyne VLP-16 User Manual, http://velodynelidar.com/docs/manuals/63-9243%20Rev%20B%20User%20Manual%20and%20Programming%20Guide,VLP-16.pdf (Accessed 20 Feb 2017).

[9] Habib, A., Jennifer Lay, and Carmen Wong. "Specifications for the Quality Assurance and Quality Control of LIDAR Systems." *Submitted to the Base Mapping and Geomatic Services of British Columbia* (2006).